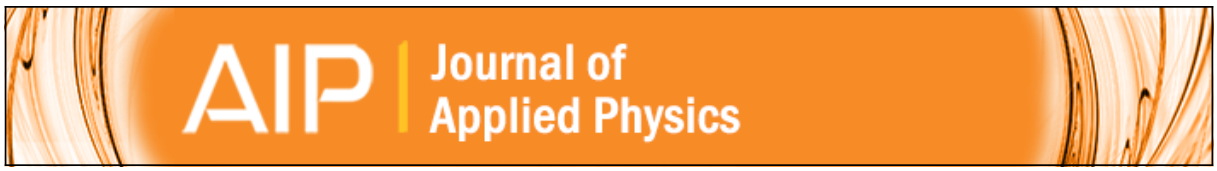

Lattice parameters and electronic structure of BeMgZnO quaternary solid solutions: Experiment and theory

M. Toporkov, D. O. Demchenko, Z. Zolnai, J. Volk, V. Avrutin, H. Morkoç, and Ü. Özgür

Citation: Journal of Applied Physics **119**, 095311 (2016); doi: 10.1063/1.4942835

View online: http://dx.doi.org/10.1063/1.4942835

View Table of Contents: http://scitation.aip.org/content/aip/journal/jap/119/9?ver=pdfcov

Published by the AIP Publishing

Lattice parameters and electronic structure of BeMgZnO quaternary solid solutions: Experiment and theory

M. Toporkov,[1] D. O. Demchenko,[2] Z. Zolnai,[3] J. Volk,[1,3] V. Avrutin,[1] H. Morkoç,[1] and Ü. Özgür[1]
[1]*Department of Electrical and Computer Engineering, Virginia Commonwealth University, Richmond, Virginia 23284, USA*
[2]*Department of Physics, Virginia Commonwealth University, Richmond, Virginia 23284, USA*
[3]*MTA EK Institute of Technical Physics and Materials Science, Budapest, Hungary*

(Received 11 December 2015; accepted 13 February 2016; published online 7 March 2016)

$Be_xMg_yZn_{1-x-y}O$ semiconductor solid solutions are attractive for UV optoelectronics and electronic devices owing to their wide bandgap and capability of lattice-matching to ZnO. In this work, a combined experimental and theoretical study of lattice parameters, bandgaps, and underlying electronic properties, such as changes in band edge wavefunctions in $Be_xMg_yZn_{1-x-y}O$ thin films, is carried out. Theoretical *ab initio* calculations predicting structural and electronic properties for the whole compositional range of materials are compared with experimental measurements from samples grown by plasma assisted molecular beam epitaxy on (0001) sapphire substrates. The measured *a* and *c* lattice parameters for the quaternary alloys $Be_xMg_yZn_{1-x}$ with $x = 0-0.19$ and $y = 0–0.52$ are within 1%–2% of those calculated using generalized gradient approximation to the density functional theory. Additionally, composition independent ternary BeZnO and MgZnO bowing parameters were determined for *a* and *c* lattice parameters and the bandgap. The electronic properties were calculated using exchange tuned Heyd-Scuseria-Ernzerhof hybrid functional. The measured optical bandgaps of the quaternary alloys are in good agreement with those predicted by the theory. Strong localization of band edge wavefunctions near oxygen atoms for BeMgZnO alloy in comparison to the bulk ZnO is consistent with large Be-related bandgap bowing of BeZnO and BeMgZnO (6.94 eV). The results in aggregate show that precise control over lattice parameters by tuning the quaternary composition would allow strain control in $Be_xMg_yZn_{1-x-y}O$/ZnO heterostructures with possibility to achieve both compressive and tensile strain, where the latter supports formation of two-dimensional electron gas at the interface. © *2016 AIP Publishing LLC*.
[http://dx.doi.org/10.1063/1.4942835]

I. INTRODUCTION

Group-IIA-oxide materials of the ZnO family have attracted a great deal of interest for UV-visible optoelectronics owing to their large bandgaps (3.3 eV for ZnO) and large exciton binding energies (60 meV for ZnO).[1,2] Alloying ZnO with BeO, MgO, and CdO allows tuning of bandgap, lattice parameters, band offsets, and spontaneous polarization. Precise control over these parameters for manipulating carrier confinement and strain-induced piezoelectric polarization is essential in many applications, particularly solar-blind photodetectors, intersubband transition devices, and heterostructures with two-dimensional electron gas (2DEG) as well as light emitting devices. However, bandgaps achievable in MgZnO and BeZnO ternaries are restricted by limited solubility of BeO and MgO in wurtzite ZnO lattice. As MgO is stable in the rocksalt phase (7.7 eV bandgap), phase segregation in MgZnO is inevitable and has been reported for Mg concentrations above 33% (corresponding wurtzite MgZnO bandgap of ~4.0 eV) for films grown at substrate temperatures of ≥600 °C.[3,4] Higher Mg contents up to 55% (corresponding wurtzite MgZnO bandgap of ~4.5 eV) could be achieved at much lower growth temperatures of 250 °C at the expense of significantly degraded material quality and tendency toward phase segregation at elevated temperatures.[5] On the other hand, in the case of BeZnO ternary (BeO having the wurtzite structure with 10.6 eV bandgap), the phase segregation is primarily driven by the large difference in covalent radii (1.22 Å for Zn and 0.96 Å for Be[6]) and has been observed for Be contents as low as 10%,[7–9] despite the relatively low growth temperatures used (400–500 °C).

To overcome the abovementioned limitations of the MgZnO and BeZnO ternaries and suppress phase segregation, the quaternary BeMgZnO alloy can be used with achievable bandgaps above 5 eV.[7,10–13] The advantage of this quaternary system is that Mg has a much larger covalent radius (1.41 Å)[6] than Be and can compensate for the large lattice mismatch between ZnO and BeO. Therefore, it is expected that by tuning the compositions of both BeO and MgO in ZnO (i.e., Be/Mg ratio), one can achieve lattice matching to ZnO, prevent phase separation, and achieve wider bandgaps.

Despite its great potential, there have been only a limited number of theoretical and experimental investigations of the quaternary BeMgZnO alloy. In this work, we performed a systematic study of bandgaps, lattice parameters, and band edge wavefunction evolution in BeMgZnO thin films, with theoretical calculations predicting their structural and electronic properties for the entire compositional range. Lattice

parameters were calculated using generalized gradient approximation (GGA) to the density functional theory (DFT), while bandgaps were calculated using exchange tuned Heyd-Scuseria-Ernzerhof (HSE06) hybrid functional. The theoretical predictions were compared with the experimental measurements for quaternary alloys with up to 19% and 52% BeO and MgO, respectively.

II. METHODS

Quaternary BeMgZnO thin films were grown on (0001) sapphire substrates using plasma assisted molecular beam epitaxy (MBE) with an RF oxygen plasma source and Knudsen cells for Zn, Be, and Mg. Pyrolytic boron nitride (PBN) crucibles were used for Zn and Mg sources and a BeO crucible for the Be source. First, a 2 nm-thick MgO buffer layer was grown at 750 °C to ensure 2D nucleation. Subsequently, a 10–15 nm thick low temperature (LT) ZnO buffer layer was grown at 300 °C and annealed at 750 °C to achieve an atomically flat surface. BeMgZnO films were deposited at $\sim 8 \times 10^{-6}$ Torr oxygen pressure, 400 W RF plasma power, and 400 °C substrate temperature, which as a set of conditions were found to be optimal for the best crystal quality with high Be incorporation (up to 19%).[7] In addition, one MgZnO layer and three BeZnO layers of various compositions were grown at the same substrate temperature of 400 °C to obtain reference lattice parameters and bandgap values for the ternary compounds. The growth rate was ~100 nm/h, and the film thicknesses are ~170 nm (determined from step profiler measurements). The compositions, lattice parameters, and bandgaps of the samples investigated here are provided in Table I.

For selected ternary and quaternary alloy samples, the compositions were determined using Ion Beam Analysis (IBA) employing Rutherford Backscattering Spectroscopy (RBS) with He+ ions (He+-RBS) and elastic backscattering spectrometry with protons (p-EBS) which provide Be content accuracy within 1–2 at. %. These experimental values were used as calibration for compositional estimations of other samples using deposition rates of binary oxides BeO, MgO, and ZnO measured by an Inficon quartz thickness monitor. It is worth mentioning that elastic proton backscattering measurements account for the total atomic concentrations in the films, regardless of the atoms' positions in the lattice.

TABLE I. The lattice parameters and bandgaps of MBE grown quaternary BeMgZnO layers with corresponding measurement errors. The compositional values are within ±1–2 at. % of Be for all samples and within ±1 at. % of Mg for Set I (near 9% Be content, varying Mg content) and within ±4 at. % of Mg for Set II (near 39% Mg content, varying Be content).

Sample	*a* parameter (Å)	*c* parameter (Å)	Bandgap (eV)
Set I: Be content near ~9%			
$Be_{0.08}Zn_{0.92}O$	3.236 ± 0.020	5.123 ± 0.001	3.34 ± 0.05
$Be_{0.11}Mg_{0.14}Zn_{0.75}O$	3.208 ± 0.007	5.099 ± 0.001	3.64 ± 0.05
$Be_{0.07}Mg_{0.33}Zn_{0.60}O$	3.220 ± 0.010	5.049 ± 0.001	4.06 ± 0.05
$Be_{0.07}Mg_{0.46}Zn_{0.47}O$	3.229 ± 0.006	5.026 ± 0.001	4.44 ± 0.05
$Be_{0.12}Mg_{0.52}Zn_{0.36}O$	3.210 ± 0.006	4.979 ± 0.001	4.58 ± 0.05
Set II: Mg content near ~39%			
$Mg_{0.39}Zn_{0.61}O$	3.269 ± 0.010	5.193 ± 0.001	3.60 ± 0.05
$Be_{0.05}Mg_{0.37}Zn_{0.58}O$	3.250 ± 0.006	5.104 ± 0.001	3.75 ± 0.05
$Be_{0.07}Mg_{0.37}Zn_{0.56}O$[a]	3.245 ± 0.006	5.079 ± 0.001	3.95 ± 0.05
$Be_{0.08}Mg_{0.39}Zn_{0.53}O$[a]	3.232 ± 0.006	5.044 ± 0.001	4.19 ± 0.05
$Be_{0.19}Mg_{0.42}Zn_{0.39}O$	3.160 ± 0.006	4.939 ± 0.001	4.62 ± 0.10

[a]Considered also as part of the set of samples with near 9% Be content.

To vary the quaternary alloy composition, the Zn and Mg source temperatures were varied in the ranges of 416–452 °C and 317–325 °C, respectively, while the Be source temperature was kept at 1150 °C for all BeZnO and BeMgZnO samples investigated here. The growth progression and to some extent the structural quality of the samples were monitored *in situ* by using Reflection High-Energy Electron Diffraction (RHEED). The out-of-plane *c* and in-plane *a* lattice parameters were deduced from X-Ray Diffraction (XRD) measurements ($Cu_{K\alpha}$ radiation) for the symmetric (0002) and skew-symmetric $(10\bar{1}3)$ reflections, respectively, using the line focus mode. The optical absorption measurements were performed using a Deuterium lamp and a SPEX 500M scanning spectrometer equipped with a photomultiplier tube. The experimental bandgaps were deducted from $(\alpha_{opt}h\nu)^2$ vs. $h\nu$ Tauc plots, where α_{opt}, the absorption coefficient, was deduced from the transmission measurement and from the measured thickness values. More detailed discussion of the sample preparation can be found in the previous reports.[7,14]

We used first principles calculations to analyze structure and electronic properties of quaternary BeMgZnO alloys. The structural properties were calculated using Perdew-Burke-Ernzerhof (PBE)[15] parameterization of the GGA[16] to the DFT. Although in most cases PBE approximation is known to slightly overestimate the lattice constants, it was found to be adequate in this study as marginal improvements were obtained using a more accurate HSE06 hybrid functional,[17] which comes with a significantly increased computational cost.

The electronic bandgaps computed by PBE, on the other hand, are significantly underestimated for the ZnO family of binaries: the PBE gaps obtained here are 4.99 eV for rock-salt MgO, 0.74 eV for ZnO, and 7.87 eV for BeO, showing mean error of 2.72 eV in comparison with the experimental values discussed below. Therefore, analysis of quaternary oxides using (semi)local approximations to the DFT is problematic. In contrast, standard HSE06 hybrid functional yields a drastically lower mean absolute error for the semiconductor bandgaps of only 0.26 eV.[18] Furthermore, in HSE06, the exchange-correlation energy contains exact Fock-type exchange part that is mixed with the (semi)local part in a ratio (standard fraction of exact exchange is 0.25) that can be adjusted to fit the experimental bandgap of a specific material. The fraction of exact exchange (0.375) adjusted to yield the experimental low temperature bandgap of 3.43 eV for ZnO[19] yields the bandgap of 10.2 eV for BeO, which is close to the experimental value of 10.6 eV,[20] and 7.72 eV for the stable rock-salt phase of MgO, close to the measured bandgap of 7.7 eV.[21] Based on the good agreement of calculated bulk binary bandgaps with experiment, a common value of 0.375 was adopted in this work for the exact exchange[22] fraction with the expectation that reasonable

bandgaps will be obtained at intermediate concentrations of Mg and Be in BeMgZnO.

All calculations were performed using supercells with 72 atoms and using Γ–point eigenvalues only, and projector augmented wave (PAW) pseudopotentials. Wurtzite lattice was used throughout the work for all alloy compositions, which leads to an additional error at high concentrations of Mg, where rock-salt crystal structure would prevail. However, in quaternary BeMgZnO alloys, the rock salt phase becomes energetically favorable for fractions of Mg exceeding 75% for alloy containing 3% of Be and 83% for alloy with 17% of Be.[13] These high concentrations of Mg are not accessible in experiment, and therefore, present purely theoretical interest at the moment. Therefore, for all data related to experimentally grown BeMgZnO alloy, and even at higher Mg and Be concentrations, the wurtzite structure is appropriate. All atomic structures were relaxed within PBE with respect to the lattice parameters a and c, c/a ratio, as well as all internal degrees of freedom, to yield forces of 0.01 eV/Å or less. The plane wave basis sets with 500 eV energy cutoff were used in PBE calculations. This allowed accurate calculations of the BeMgZnO crystal structure. The electronic properties were computed for relaxed crystal structures using HSE06 hybrid functional with 0.375 fraction of exact exchange and 400 eV energy cutoff. The exchange range separation parameter in HSE06 was kept at 0.2 $Å^{-1}$.

III. RESULTS AND DISCUSSION

Table II summarizes the calculated bandgaps and lattice parameters for the binaries and compares them with theoretical results obtained by several widely used methods and

TABLE II. Calculated in-plane (a) and out-of-plane (c) lattice parameters and bandgaps for the binaries ZnO, MgO, and BeO (note that u = 3/8 = 0.375 in the ideal wurtzite structure) compared with representative experimental values.

		Theory				Experiment			
		a (Å)	c (Å)	U	E_g (eV)	a (Å)	c (Å)	u	E_g (eV)
ZnO (wz)	This work	3.30	5.285	0.378	3.43 [HSE06-0.375]	3.252	5.203		3.26
		3.166[a]	5.070[a]	0.380[a]	2.48[b] [HSE06-0.25]	(3.248–3.250)[e]	(5.204–5.241)[e]	(0.382–0.386)[e]	3.43 (LT)
					2.12–3.2[c] [GW]				
					0.74[d] [GGA]			0.382[f]	
MgO (wz)	This work	3.32	5.056	0.386	5.87 [HSE06-0.375]	3.283[g]	5.095[g]	0.388[g]	5.88[h]
		3.221[a]	5.040[a]	0.386[a]	5.21[b] [HSE06-0.25]				
					7.16[i] [GW]				
					3.78[j] [LDA]				
MgO (rock-salt)	This work	4.17	N/A	N/A	7.72 [HSE06-0.375]		N/A	N/A	
		4.21[k]			6.67[b] [HSE06-0.25]	4.207[n]			7.77[p]
					8.2–9.16[l] [GW]	4.211[o]			7.7[q]
					4.34[m] [GGA]				
BeO (wz)	This work	2.72	4.393	0.378	10.20 [HSE06-0.375]				
		2.738[r]	4.449[r]	0.377[s]	10.09[t] [HSE06-0.25]	2.698[w]	4.3776[w]	0.378[x]	10.63[y]
					10.8[u] [GW]				
					8.49[v] [GGA]				

[a]LDA + U to DFT with ultrasoft pseudopotentials.[27]
[b]Untuned HSE06 with fraction of exact exchange equal 0.25.[23]
[c]Various GWs.[28]
[d]GGA.[29]
[e]XRD and energy-dispersive X-ray spectroscopy (EDX).[1]
[f]Powder neutron diffraction.[30]
[g]Extrapolation of the experimental data.[27]
[h]Extrapolation of the experimental data.[25]
[i]G_0W_0.[23]
[j]LDA to DFT.[24]
[k]GGA(PAW) to DFT.[26]
[l]Various GWs.[31]
[m]GGA(PBE) to DFT.[32]
[n]XRD.[33]
[o]XRD.[34]
[p]Reflectance.[35]
[q]Reflectance.[21]
[r]GGA(PBE) to DFT.[36]
[s]DFT in the framework of the periodic linear combination of atomic orbitals (LCAOs) approximation.[37]
[t]Untuned HSE06 with fraction of exact exchange equal 0.25.[38]
[u]GW.[39]
[v]GGA(PBE) to DFT.[38]
[w]XRD.[40]
[x]Neutron and γ-ray diffraction.[41]
[y]Reflectance.[20]

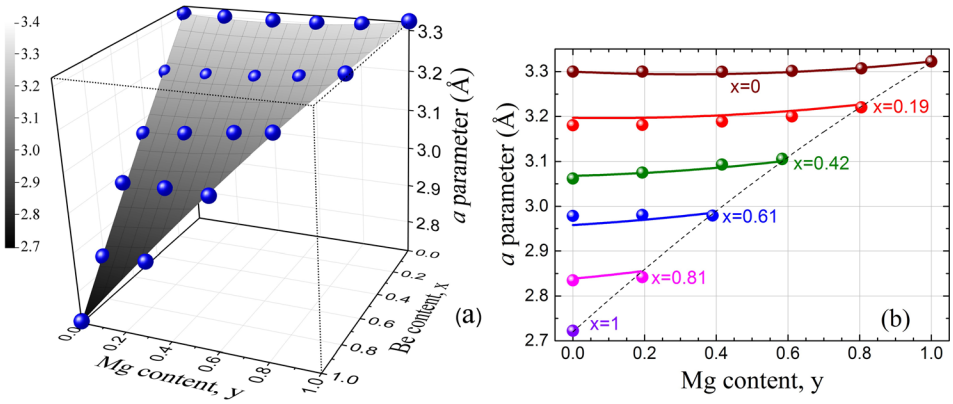

FIG. 1. (a) Calculated *a* lattice parameters of $Be_xMg_yZn_{1-x-y}O$ as a function of Be and Mg contents. Solid circles represent calculated values using PBE-DFT, and the surface is a fit using Equation (1), which provided the bowing parameters listed in Table III. (b) Computed a lattice parameter values as a function of Mg content for different Be compositions. The solid lines are the corresponding sections from the surface fit in (a). The dashed line corresponds to $Be_{1-y}Mg_yO$ ternary alloy.

representative experimental values. It is well known that local/semilocal local density approximation (LDA)/GGA underestimates the bandgaps in oxides, sometimes by several eV. Although standard HSE06 hybrid functional (fraction of exact exchange equal to 0.25) provides significant improvement, it still underestimates the bandgaps of bulk ZnO (2.48 eV), BeO (10.09 eV), and MgO (6.67 eV). On the other hand, GW (Green's function G and the screened Coulomb interaction W) quasiparticle calculations, often considered to be more accurate, are significantly more computationally demanding compared with hybrid functional calculations, and in some cases they can overestimate the bandgaps, as for BeO and MgO (see Table II). Therefore, HSE06 hybrid functional calculations, with exact exchange fraction tuned to match the experimental bandgap of ZnO, are the most practical, producing results in excellent agreement with experiment at moderate computational cost. The accurate prediction of rock-salt MgO bandgap provides confidence in the bandgap value for the quasi-stable wurtzite MgO. Moreover, the bandgap for wurtzite MgO has been theoretically predicted using GW calculations to be 7.16 eV (Ref. 23) or 6.34 eV (Ref. 24) (the latter value was obtained by using the correction of 2.56 eV derived from the calculation of rocksalt MgO). A linear extrapolation of the experimental bandgaps of wurtzite MgZnO alloy[25] suggests a value in the vicinity of 5.9 eV, consistent with our result. Similarly, in-plane and out-of-plane lattice parameters of a = 3.283 Å and c = 5.095 Å, respectively, reported for wurtzite MgO based on extrapolation of experimental results on MgZnO,[26] are reasonably well-reproduced by the GGA to DFT calculations reported here (Table II).

Figure 1(a) displays the in-plane lattice parameters for $Be_xMg_yZn_{1-x-y}O$ solid solution calculated using PBE approximation to DFT for the full range of compositions. The directly computed data (solid spheres for select compositions) exhibit bowing and can be represented by the polynomial form[42]

$$a_{BeMgZnO}(x,y) = xa_{BeO} + ya_{MgO} + (1-x-y)a_{ZnO} - b_{BeZnO}x(1-x) - b_{MgZnO}y(1-y) - b_{xy}xy, \quad (1)$$

where b_{BeZnO}, b_{MgZnO}, and $b_{xy} = b_{BeZnO} - b_{MgZnO} - b_{BeMgO}$ are the bowing parameters that are independent of the composition.[43] The surface plot in Figure 1(a) is the fit using Equation (1). As will be discussed below, computed *c* lattice parameters and the bandgaps can also be represented by Equation (1) with *a* replaced by the corresponding parameter. Additionally, since our calculations cover the entire range of compositions, this interpolation formula for quaternary $Be_xMg_yZn_{1-x-y}O$ also yields the bowing parameters for ternary compounds that can be used to explain the properties of the corresponding ternary alloys. Note that there are different methods used across the literature with varying bowing equations, different definitions of bowing parameters, and their dependence on the composition of the quaternary alloy making it often difficult to compare the bowing parameters reported.

The bowing parameters obtained from the fits using Equation (1) are provided in Table III. For convenience, Figure 1(b) displays the dependence of *a* lattice parameter on Mg content for various fixed Be contents in BeMgZnO alloys. As also shown in Table II, the *a* parameter of wurtzite MgO is very close to that of ZnO due to relatively small difference in covalent radii (1.22 Å for Zn and 1.41 Å for Mg).[6] On the other hand, due to the smaller covalent radius of Be (0.96 Å)[6] compared with Zn, the in-plane lattice parameter of BeO is substantially smaller than that of ZnO. The bowing of the surface in Figure 1(a) is relatively small despite the wide range of the lattice parameter variation in BeMgZnO. By choosing proper Be and Mg content, it is possible to achieve in-plane lattice parameter larger (by a small amount) or smaller than that of ZnO. The latter one is very important in achieving tensile strain in the barrier layer of Zn-polar BeMgZnO/ZnO heterostructure, which yields to the proper

TABLE III. Bowing parameters for the quaternary BeMgZnO alloy calculated in this work and reported in literature.

		a (Å)	*c* (Å)	Bandgap (eV)
b_{BeZnO}	This work	−0.043	−0.043	6.94
		Linear[a]	Linear[a]	5.6[a]
		...	…	4.5[b]
b_{MgZnO}	This work	0.061	−0.172	0.237
		0.04167[c]	−0.1333[c]	…
b_{xy}	This work	−0.140	0.427	−2.79

[a]GGA(PBE) to DFT.[36]
[b]Absorption measurements on RF magnetron sputtered BeZnO.[46]
[c]GGA(PAW) to DFT.[26]

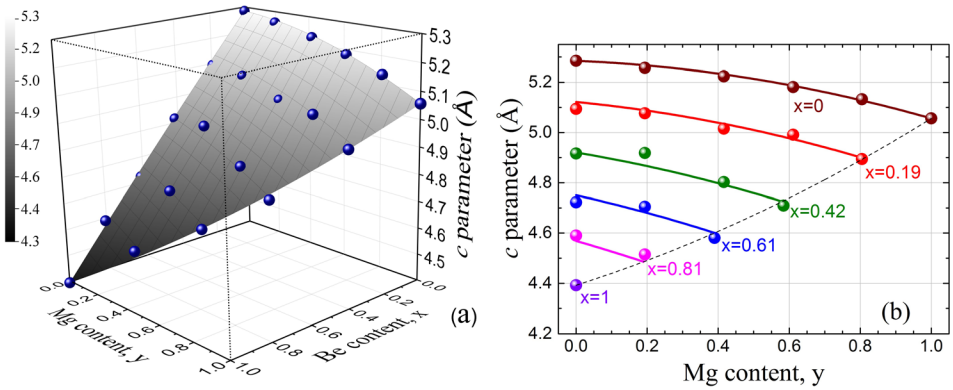

FIG. 2. (a) Calculated c lattice parameters of $Be_xMg_yZn_{1-x-y}O$ as a function of Be and Mg contents. Solid circles represent calculated values using PBE-DFT, and the surface is a fit using Equation (1) which provided the bowing parameters listed in Table III. (b) Computed c lattice parameter values as a function of Mg content for different Be compositions. The solid lines are the corresponding sections from the surface fit in (a). The dashed line corresponds to $Be_{1-y}Mg_yO$ ternary alloy.

sign of piezoelectric polarization and results in high 2DEG density near the interface. For Zn-polar $Be_xMg_{0.2}Zn_{0.8-x}O$/ZnO heterostructures, even 5% of Be should provide sufficient piezoelectric polarization to generate 2DEG sheet density above $10^{13}\,cm^{-2}$. The tensile strain required in the barrier layer for 2DEG generation cannot be achieved with Zn-polar MgZnO/ZnO heterostructure.

Figure 2 shows the calculated out-of-plane c lattice parameters of BeMgZnO (solid spheres) and the fit (surface) obtained using Equation (1). Bowing of the c lattice parameter is observed to be significantly larger than that of the a parameter due to the fact that the incorporations of Mg and Be have opposite effects on the in-plane lattice parameter (reducing with Be, increasing with Mg), while the out-of-plane lattice parameter of BeMgZnO reduces with increasing both Be and Mg content.

Figure 3(a) presents the theoretically calculated bandgap values using tuned HSE06 hybrid functional with the fraction of exact exchange 0.375 (solid spheres) and the fit using Equation (1) (the surface fit) for the entire range of BeMgZnO compositions. Figure 3(b) shows the computed bandgaps as a function of Mg content for different Be contents. The bandgap bowing for ternary MgZnO compound is relatively small, while that for BeZnO is clearly noticeable in Figure 3(a).

The theoretical methods used here were validated by comparing the calculated lattice parameters and bandgaps with those measured for MBE-grown quaternary layers. Figures 4(a) and 4(b) compare the calculated a and c lattice parameters, respectively, of BeMgZnO quaternary solid solutions with experimental values. It is worth noting that incorporation of Be, which has small covalent radius on the Zn lattice sites, partially compensates the lattice expansion caused by Mg and permits attainment of BeMgZnO layers containing up to approximately 50% Mg.[7] As GGA to DFT in most cases is known to overestimate the lattice parameters by 1%–2%, as expected, the calculated values are larger than the measured ones by about 0.04 Å and 0.08 Å for a and c parameters, respectively. This discrepancy also partially originates from slight variations in the actual Be and Mg atomic contents (see Table I) from the plotted 9% and 39%, respectively, as well as the error in measurement of the lattice parameters (see Table I) and the compositions.[14] The error bars shown in Figure 4 represent the corresponding overall confidence limits. The measurement error results partially from alloy XRD peak broadening and use of the relatively weak and broad low-temperature ZnO XRD peak as the reference position for asymmetric XRD scans. It is observed in Figure 4(a) that $Be_{0.09}Mg_yZn_{0.91-y}O$ samples (blue circles) exhibit larger scatter in the measured in-plane lattice parameter around the expected trend compared with the $Be_xMg_{0.4}Zn_{0.6-y}O$ samples (red stars). The main source of error in this case is the deviation of the actual Be content from the plotted 9% as a small change in the Be molar content results in a significant change in the in-plane lattice parameter. Nevertheless, despite the rigid shift due to slight overestimation of the predicted lattice parameters, the theoretical model satisfactorily predicts the lattice parameters of the quaternary alloy.

Figure 5 compares the calculated and measured bandgaps for $Be_{0.09}Mg_yZn_{0.91-y}O$ solid solutions. The difference between theoretically predicted electronic bandgaps and experimentally determined optical bandgaps is 0.14–0.32 eV for Set I (samples with near 9% Be but varying Mg content) and higher for Set II (samples with near 39% Mg but varying

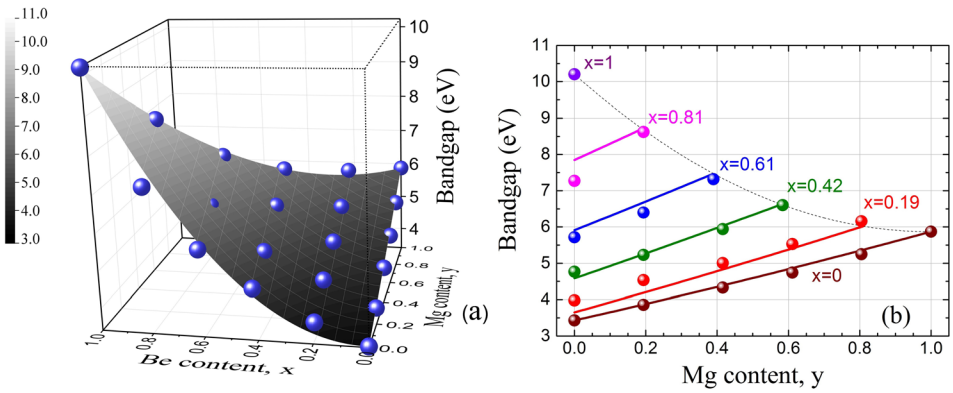

FIG. 3. (a) Calculated bandgaps of $Be_xMg_yZn_{1-x-y}O$ as a function of Be and Mg contents. Solid circles represent calculated values using the exchange tuned HSE06 hybrid functional, and the surface is a fit using Equation (1), which provided the bowing parameters listed in Table III. (b) Computed bandgaps as a function of Mg content for different Be compositions. The solid lines are the corresponding sections from the surface fit in (a). The dashed line corresponds to $Be_{1-y}Mg_yO$ ternary alloy.

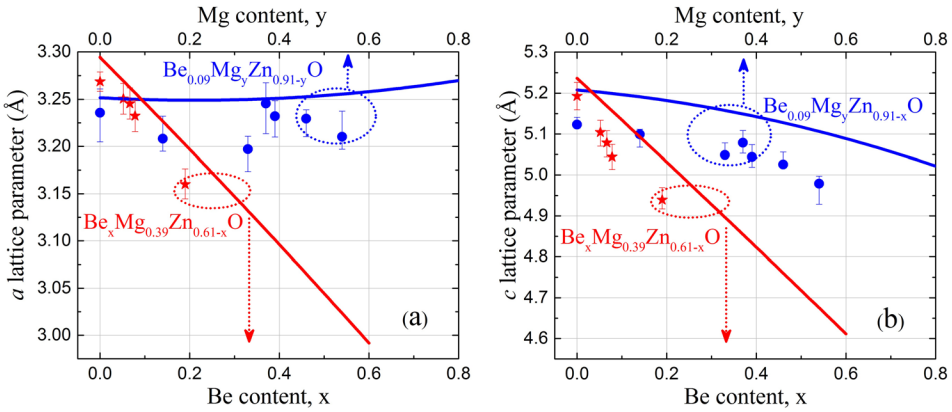

FIG. 4. (a) In-plane and (b) out-of-plane lattice parameters of $Be_xMg_{0.39}Zn_{0.61-x}O$ (red curve for theory and red stars for experiment) and $Be_{0.09}Mg_yZn_{0.91-y}O$ (blue curve for theory and blue circles for experiment) as functions of Be and Mg contents, respectively. The error bars indicate the confidence limits originating from slight variations in the actual Be and Mg atomic contents from the plotted 9% and 39%, respectively, as well as the error in measurement of the lattice parameters (see Table I) and the compositions.

Be content). The large deviation for Set II when Be content is 8% or lower may be attributed to possible segregation of the Mg-rich phase, which is characteristic to high Mg content MgZnO. Phase segregation would also take place in the quaternary alloy with Be concentration insufficient to compensate the tensile strain caused by large Mg content.[13] As a result, effectively lower Mg content remains in the wurtzite lattice, which would be revealed as lower optical bandgap. It should be noted that XRD measurements are not sensitive enough to reveal any secondary phase. Moreover, as the effect of Mg incorporation on the lattice parameters is smaller than that of Be, the effect of phase segregation may not be noticeable, particularly also due to broad XRD peaks.[7]

The discrepancy between calculated and measured bandgaps shown in Figure 5 is also associated with neglecting temperature expansion of the lattice, temperature dependence of electron-phonon coupling, and excitonic effects

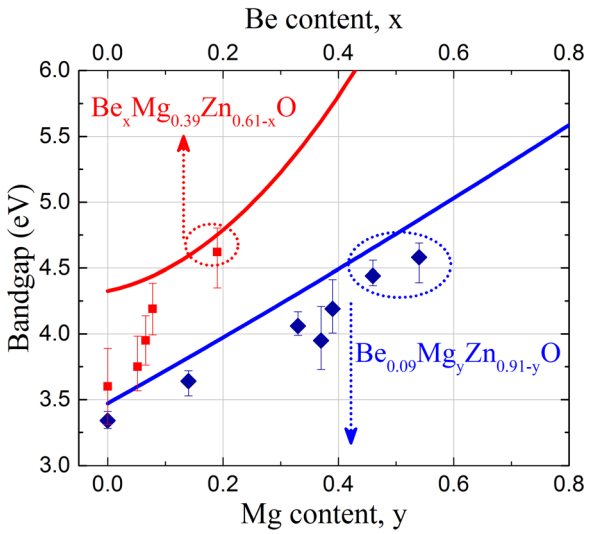

FIG. 5. Bandgaps of $Be_{0.09}Mg_yZn_{0.91-y}O$ and $Be_xMg_{0.39}Zn_{0.61-x}O$ solid solutions calculated using tuned HSE06 (solid lines) compared with experiment (symbols). The large deviation between experimental and theoretical values for $Be_xMg_{0.39}Zn_{0.61-x}O$ for Be content below 10% is attributed to possible segregation of Mg-rich phase. On the other hand, for samples with relatively high Be content, Be can suppress phase segregation of Mg-rich phase and thus increase incorporation of Mg to the wurtzite lattice of BeMgZnO alloy due to compensation of the tensile strain resulting from large Mg content. The compositions of all $Be_xMg_{0.39}Zn_{0.61-x}O$ samples are estimated based on flux measurements and thus show accumulative amount of Be and Mg in the quaternary layers.

in *ab initio* calculations. The hybrid functional method of calculations was tuned to yield the bandgap that matches the measured low-temperature ZnO bandgap of 3.43 eV (obtained from the 3.37 eV low temperature emission of A-exciton plus the exciton binding energy E_B^X of 60 meV), higher than the excitonic bandgap measured at room temperature (3.26 eV). Similarly, for MgO and BeO, increasing temperature from 77 K to 300 K results in bandgap shrinkage of about 0.2 eV (Ref. 35) and 0.1 eV,[20] respectively. Thus, the combined effects of lattice expansion and temperature dependence of electron-phonon coupling on the bandgap of BeMgZnO alloy can account for variations in the range of 0.1 eV to 0.2 eV. The decrease in bandgap due to the excitonic effect only is 80 meV in rocksalt MgO,[35] and the reported excitonic binding energy of wurtzite MgZnO does not vary from that of ZnO by more than 10 meV for Mg content up to 29%.[19,44] The excitonic binding energy measured for BeO, on the other hand, is significantly higher (0.17 eV). Therefore, for ternary BeZnO and quaternary BeMgZnO alloys, the exciton binding energy is expected to fall within the range determined by ZnO and BeO exciton binding energies, i.e., 0.06–0.17 eV. These estimates suggest that the systematic difference between the calculated and measured bandgaps in BeMgZnO alloys is mainly due to excitonic effects and temperature dependent renormalization of the bandgap, unaccounted for in the theoretical method. When all these effects are considered, the satisfactory prediction of $Be_{0.09}Mg_yZn_{0.91-y}O$ bandgap by the theory suggests that the use of the HSE hybrid functional in our calculations yields the correct bandgaps for both constituent binaries and their solid solutions. Thus, the bowing parameters provided in Table III are expected to be well representative. It should be noted, however, that although the solubility limits in the BeO-MgO-ZnO system have not yet been explored in detail, growing single-phase material with large Mg and Be content while maintaining the material quality may be extremely challenging or even impossible because of strong tendency for phase segregation observed for MgZnO and BeZnO ternaries.

Table III compares the bowing parameters computed here for the quaternary BeMgZnO system, with those of the ternary alloy subsystems, BeZnO and MgZnO, from literature. We obtain negative and relatively small values for BeZnO bowing of −0.043 Å for both *a* and *c* lattice

parameters. The in-plane lattice bowing parameter for MgZnO is 0.061 Å and out-of-plane lattice bowing is negative but larger in the absolute value, −0.172 Å. Among the ternaries involved, MgZnO has been explored extensively both experimentally and theoretically, whereas BeZnO has received limited attention, and BeMgO almost no consideration at all due to difficulty of growth. Shimada *et al.*[26] calculated structural properties of MgZnO alloy using GGA to DFT with PAW pseudopotentials and reported lattice bowing parameters similar to ours. The observed nonlinearity of the lattice parameters was attributed to difference in the chemical bonding between rocksalt MgO and wurtzite ZnO. In regard to the effect of Be incorporation, the calculations predict relatively small bowing parameters for the compositional dependences of the lattice parameters in BeZnO, as shown in Table III. Using GGA, Su *et al.*[45] performed DFT calculations of lattice parameters of wurtzite BeMgZnO for selected compositions; however, no bowing was reported. The bowing parameters b_{a_BeZnO} and b_{c_BeZnO} determined here are relatively small and have not been reported to date, in part due to the complications associated with precise determination of the Be content, with the measurement error being higher than the effect of bowing itself. In addition, experimental studies of BeZnO for a wide range of compositions are challenging because of phase segregation observed for the solid solutions with both low (more than ∼10% Be) and high Be (less than ∼75% Be) content.[8]

In regard to bandgap bowing, we obtain relatively large BeZnO bowing of 6.94 eV and relatively small MgZnO bowing of 0.237 eV, which shows that the bowing parameters increase with the size difference of the constituents. Shi and Duan[42] calculated bandgaps of zinc blende BeMgZnO using LDA to DFT and reported large and composition dependent bandgap bowing parameters. However, the composition dependence does not allow comparison with the results presented here. Ding *et al.*[36] reported theoretical investigation of the bandgap of ternary BeZnO with a bowing parameter of 5.6 eV. The bandgap bowing parameter b_{Eg_BeZnO} has also been reported experimentally (4.5 eV in Ref. 46) but is lower than the theoretically predicted value most likely due to low range of available Be compositions and low crystal quality. It should also be noted that, in our case, the calculated bowing parameters are independent of composition, indicating that the symmetry of the wave functions does not change significantly due to incorporation of Mg and Be to the lattice of ZnO to form the quaternary BeMgZnO alloy.

In order to understand the evolution of the lattice and the bandgap of the BeMgZnO alloys with the increasing Be and Mg contents, Figure 6 shows the crystal structures along with the isosurfaces of the electron density corresponding to the valence band maxima (VBM) for bulk ZnO [Figure 6(a)] and BeMgZnO alloy with 19% of Be and 42% of Mg [Figure 6(b)]. Significant structural distortions due to lattice relaxation are observed in the BeMgZnO alloy. Bond lengths between Mg and O atoms and Zn and O atoms are similar and on average about ∼2 Å, while Be-O bonds are significantly shorter, on average ∼1.7 Å. Due to a large BeO formation enthalpy ($\Delta_f H^0 = -6.316$ eV),[47] Be-O bonding is significantly stronger than that of Zn-O ($\Delta_f H^0 = -3.632$ eV),[47] which is another

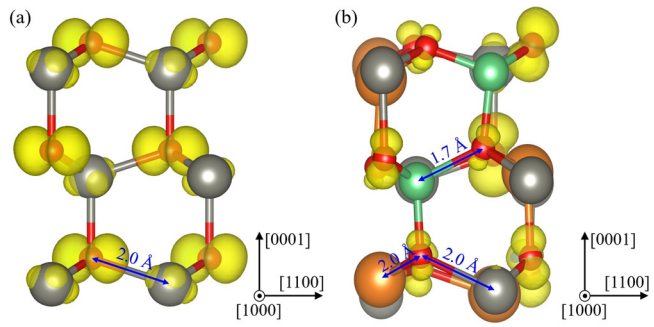

FIG. 6. HSE06 calculated band-decomposed charge densities for valence band maximum (VBM) for (a) bulk ZnO and (b) $Be_{0.19}Mg_{0.42}Zn_{0.39}O$. The isosurfaces (yellow) are set at 6% of the maximum value. In each case, a small fragment of the super cell is shown for clarity, with vertical direction corresponding to wurtzite (0001) axis. Zn, Mg, Be, and O atoms are represented by large gray, large orange, medium green, and small red spheres.

reason for the decrease in the lattice constant when admixing Be to ZnO. At the same time, MgO has formation enthalpy ($\Delta_f H^0 = -6.235$ eV)[47] similar to BeO; however, larger atom size leads to Mg-O bond length being similar to that of ZnO.

As shown in Figure 6, electron densities are localized on oxygen atoms away from the formal bond centers. This shift is quite pronounced in HSE06 due to partial correction of the self-interaction error for the oxygen 2*p*-derived states, which make up most of the upper part of the valence band in both ZnO and BeMgZnO. Electron densities show stronger localization in BeMgZnO alloy compared with bulk ZnO. Particularly, the VBM orbitals localized on oxygen coordinated by Mg atoms tend to be more localized, compared with those coordinated by zinc [Figure 6(b)]. These changes in the wavefunction with increasing concentration of Mg and Be are related to the bandgap bowing discussed above. Larger bowing is usually accompanied by a stronger wavefunction localization. For example, in $Al_xGa_{1-x}N$ alloys, the similarity between Ga and Al atoms leads to small bowing and weak wavefunction localization.[48] On the other hand, in $In_xGa_{1-x}N$, the stronger wavefunction localization also leads to larger bandgap bowing.[49] In the case of BeMgZnO alloys, the wavefunction localization as a result of alloying is significant, which explains the observed bandgap bowing. At the same time, the compensating effect of substituting Be and Mg on Zn sites leads to relatively small average changes in metal-oxygen bond lengths, leading to small bowing in lattice parameters.

In order to quantify the overall wavefunction localization in BeMgZnO, we calculate participation ratio (PR) for conduction band minima (CBM) and VBM wavefunctions $V\int|\psi(\mathbf{r})|^4 d\mathbf{r}$.[48] The PR is equal to 1 for a constant function and has larger value for any spatially varying function, with larger values for stronger localization. Compared with GGA, the wavefunctions computed with HSE06 are usually more localized, resulting in larger bandgap bowing. Table IV presents computed PR values normalized to the most delocalized state in our calculations, which is bulk ZnO CBM state. In all alloy configurations, both CBM and VBM wavefunctions are more localized, compared with bulk ZnO. Admixing Be atoms into the alloy shows stronger

TABLE IV. Participation ratios for the CBM and VBM wavefunctions in bulk ZnO and $Be_xMg_yZn_{1-y}O$ alloys, normalized to the bulk ZnO CBM. Larger values correspond to stronger localization of the wavefunction.

	CBM	VBM
Bulk ZnO	1.0	5.92
$Mg_{0.42}Zn_{0.58}O$	1.13	7.22
$Be_{0.19}Zn_{0.81}O$	1.35	7.62
$Be_{0.19}Mg_{0.42}Zn_{0.39}O$	1.36	9.00

localization effect, where 19% of Be produces similar wavefunction PR values as 42% of Mg atoms in the alloy. Since the PRs for VBM increase by a factor of 1.5 from ZnO to $Be_{0.19}Mg_{0.42}Zn_{0.39}O$ alloy, indicating significant changes in the band edge wavefunctions, the calculated values of bandgap bowing are significant as well. Enhanced localization also usually indicates stronger interatomic bonding, which also leads to increased bandgap bowing.

IV. CONCLUSIONS

In conclusion, we performed a systematic experimental and theoretical study of lattice parameters and bandgaps of quaternary BeMgZnO alloy for the whole range of compositions. The calculations using exchange tuned HSE06 hybrid functional (exchange fraction of 0.375) are in good agreement with the experimental data for MBE grown samples containing up to about 19% Be and 52% Mg in quaternary BeMgZnO alloy. The *a* and *c* lattice parameters were calculated within 1%–2% accuracy in comparison with experimentally observed values. The effect of BeO content on the *a* lattice parameter is much stronger than that of MgO due to larger difference of lattice parameter of the former with ZnO. Further offset of 0.14–0.32 eV for $Be_{0.09}Mg_yZn_{0.91-y}O$ and higher for $Be_xMg_{0.39}Zn_{0.61-x}O$ (due to possible phase segregation) between theoretically predicted and measured bandgaps (in the available compositional range) is attributed to the temperature expansion of the lattice, temperature dependence of electron-phonon coupling, and excitonic effects. Composition independent bowing parameters were determined for ternary BeZnO and MgZnO alloys: $b_{Eg\_BeZnO} = 6.94\,eV$ and $b_{Eg\_MgZnO} = 0.237\,eV$ for bandgaps, and $b_{a\_BeZnO} = -0.043$ Å, $b_{a\_MgZnO} = -0.172$ Å and $b_{c\_BeZnO} = -0.043$ Å, $b_{c\_MgZnO} = 0.061$ Å for *a*-lattice and *c*-lattice parameters, respectively. The large bandgap bowing b_{Eg_BeZnO} correlates with strong localization of both CBM and VBM wavefunctions in BeMgZnO alloy, compared with bulk ZnO. Finally, it is important to note that by using BeMgZnO alloy as a top barrier layer on Zn-polar ZnO, it is possible to achieve both tensile and compressive strain, where former cannot be achieved with MgZnO. This is advantageous to generate high density 2DEG by utilizing piezoelectric polarization for future generation (Be,Mg)ZnO/ZnO heterostructure field effect transistors.

ACKNOWLEDGMENTS

This work was funded by the Air Force Office of Scientific Research under the program management of Dr. Kenneth Goretta.

[1]H. Morkoç and Ü. Özgür, *Zinc Oxide: Fundamentals, Materials and Device Technology* (Wiley-VCH, Weinheim, 2009).
[2]Ü. Özgür, Y. I. Alivov, C. Liu, A. Teke, M. A. Reshchikov, S. Doğan, V. Avrutin, S.-J. Cho, and H. Morkoc¸, J. Appl. Phys. **98**, 041301 (2005).
[3]A. Ohtomo, M. Kawasaki, T. Koida, K. Masubuchi, H. Koinuma, Y. Sakurai, Y. Yoshida, T. Yasuda, and Y. Segawa, Appl. Phys. Lett. **72**, 2466 (1998).
[4]A. K. Sharma, J. Narayan, J. F. Muth, C. W. Teng, C. Jin, A. Kvit, R. M. Kolbas, and O. W. Holland, Appl. Phys. Lett. **75**, 3327 (1999).
[5]X. Du, Z. Mei, Z. Liu, Y. Guo, T. Zhang, Y. Hou, Z. Zhang, Q. Xue, and A. Y. Kuznetsov, Adv. Mater. **21**, 4625 (2009).
[6]B. Cordero, V. Gómez, A. E. Platero-Prats, M. Revés, J. Echeverría, E. Cremades, F. Barragán, and S. Alvarez, Dalton Trans. **2008**, 2832.
[7]M. Toporkov, V. Avrutin, S. Okur, N. Izyumskaya, D. Demchenko, J. Volk, D. J. Smith, H. Morkoç, and Ü. Özgür, J. Cryst. Growth **402**, 60 (2014).
[8]M. Chen, Y. Zhu, L. Su, Q. Zhang, A. Chen, X. Ji, R. Xiang, X. Gui, T. Wu, B. Pan, and Z. Tang, Appl. Phys. Lett. **102**, 202103 (2013).
[9]D. Ye, Z. Mei, H. Liang, Y. Liu, A. Azarov, A. Kuznetsov, and X. Du, J. Phys. D: Appl. Phys. **47**, 175102 (2014).
[10]C. Yang, X. M. Li, Y. F. Gu, W. D. Yu, X. D. Gao, and Y. W. Zhang, Appl. Phys. Lett. **93**, 112114 (2008).
[11]L. Su, Y. Zhu, Q. Zhang, M. Chen, X. Ji, T. Wu, X. Gui, B. Pan, R. Xiang, and Z. Tang, J. Phys. D: Appl. Phys. **46**, 245103 (2013).
[12]C. Yang, X. M. Li, X. D. Gao, X. Cao, R. Yang, and Y. Z. Li, J. Cryst. Growth **312**, 978 (2010).
[13]L. Su, Y. Zhu, D. Yong, M. Chen, X. Ji, Y. Su, X. Gui, B. Pan, R. Xiang, and Z. Tang, ACS Appl. Mater. Interfaces **6**, 14152 (2014).
[14]Z. Zolnai, M. Toporkov, J. Volk, D. O. Demchenko, S. Okur, Z. Szabó, Ü. Özgür, H. Morkoç, V. Avrutin, and E. Kótai, Appl. Surf. Sci. **327**, 43 (2015).
[15]J. P. Perdew, K. Burke, and M. Ernzerhof, Phys. Rev. Lett. **77**, 3865 (1996).
[16]J. P. Perdew, Phys. Rev. Lett. **55**, 1665 (1985).
[17]J. Heyd, G. E. Scuseria, and M. Ernzerhof, J. Chem. Phys. **118**, 8207 (2003).
[18]M. Marsman, J. Paier, A. Stroppa, and G. Kresse, J. Phys.: Condens. Matter **20**, 064201 (2008).
[19]M. D. Neumann, C. Cobet, N. Esser, B. Laumer, T. A. Wassner, M. Eickhoff, M. Feneberg, and R. Goldhahn, J. Appl. Phys. **110**, 013520 (2011).
[20]D. M. Roessler, W. C. Walker, and E. Loh, J. Phys. Chem. Solids **30**, 157 (1969).
[21]*Handbook of Optical Constants of Solids*, edited by E. D. Palik and G. Ghosh (Academic Press, San Diego, 1998).
[22]J. Betancourt, J. J. Saavedra-Arias, J. D. Burton, Y. Ishikawa, E. Y. Tsymbal, and J. P. Velev, Phys. Rev. B **88**, 085418 (2013).
[23]Q. Yan, P. Rinke, M. Winkelnkemper, A. Qteish, D. Bimberg, M. Scheffler, and C. G. Van de Walle, Appl. Phys. Lett. **101**, 152105 (2012).
[24]S. Limpijumnong and W. R. L. Lambrecht, Phys. Rev. B **63**, 104103 (2001).
[25]K. Koike, K. Hama, I. Nakashima, G. Takada, K. Ogata, S. Sasa, M. Inoue, and M. Yano, J. Cryst. Growth **278**, 288 (2005).
[26]K. Shimada, N. Takahashi, Y. Nakagawa, T. Hiramatsu, and H. Kato, Phys. Rev. B **88**, 075203 (2013).
[27]S.-H. Jang and S. F. Chichibu, J. Appl. Phys. **112**, 073503 (2012).
[28]M. Shishkin and G. Kresse, Phys. Rev. B **75**, 235102 (2007).
[29]F. Oba, A. Togo, I. Tanaka, J. Paier, and G. Kresse, Phys. Rev. B **77**, 245202 (2008).
[30]E. H. Kisi and M. M. Elcombe, Acta Crystallogr., Sect. C: Struct. Chem. **45**, 1867 (1989).
[31]M. Shishkin, M. Marsman, and G. Kresse, Phys. Rev. Lett. **99**, 246403 (2007).
[32]J. Heyd, J. E. Peralta, G. E. Scuseria, and R. L. Martin, J. Chem. Phys. **123**, 174101 (2005).
[33]C. F. Klingshirn, A. Waag, A. Hoffmann, and J. Geurts, *Zinc Oxide: From Fundamental Properties Towards Novel Applications* (Springer, Heidelberg, London, 2010).
[34]O. Madelung, in*II-VI-VII Compd. Semimagn. Compd*., edited by U. Rössler and M. Schulz (Springer-Verlag, Berlin/Heidelberg, 1999), pp. 1–6.
[35]D. M. Roessler and W. C. Walker, Phys. Rev. **159**, 733 (1967).
[36]S. F. Ding, G. H. Fan, S. T. Li, K. Chen, and B. Xiao, Physica B **394**, 127 (2007).
[37]B. Amrani, F. E. H. Hassan, and H. Akbarzadeh, J. Phys.: Condens. Matter **19**, 436216 (2007).

[38]L. Shi, Y. Qin, J. Hu, Y. Duan, L. Qu, L. Wu, and G. Tang, EPL **106**, 57001 (2014).
[39]E. L. Shirley, J. A. Soininen, and J. J. Rehr, in *Opt. Constants Mater. Uv X-Ray Wavel.*, edited by R. Soufli and J. F. Seely (Spie-Int Soc Optical Engineering, Bellingham, 2004), pp. 125–137.
[40]R. M. Hazen and L. W. Finger, J. Appl. Phys. **59**, 3728 (1986).
[41]J. W. Downs, F. K. Ross, and G. V. Gibbs, Acta Crystallogr., Sect. B: Struct. Sci., Cryst. Eng. Mater. **41**, 425 (1985).
[42]H.-L. Shi and Y. Duan, Eur. Phys. J. B **66**, 439 (2008).
[43]F. Wang, S.-S. Li, J.-B. Xia, H. X. Jiang, J. Y. Lin, J. Li, and S.-H. Wei, Appl. Phys. Lett. **91**, 061125 (2007).
[44]R. Schmidt, B. Rheinländer, M. Schubert, D. Spemann, T. Butz, J. Lenzner, E. M. Kaidashev, M. Lorenz, A. Rahm, H. C. Semmelhack, and M. Grundmann, Appl. Phys. Lett. **82**, 2260 (2003).
[45]X. Su, P. Si, Q. Hou, X. Kong, and W. Cheng, Physica B **404**, 1794 (2009).
[46]J. H. Yu, D. S. Park, J. H. Kim, T. S. Jeong, C. J. Youn, and K. J. Hong, J. Mater. Sci. **45**, 130 (2010).
[47]J. A. Dean and N. A. Lange, *Lange's Handbook of Chemistry*, 15th ed. (McGraw-Hill, New York, 1999).
[48]B. Lee and L.-W. Wang, Phys. Rev. B **73**, 153309 (2006).
[49]B. Lee and L. W. Wang, J. Appl. Phys. **100**, 093717 (2006).